Journal of Luminescence 216 (2019) 116717

Contents lists available at ScienceDirect

Journal of Luminescence

journal homepage: www.elsevier.com/locate/jlumin

Emission dynamics of GaN-based blue resonant-cavity light-emitting diodes

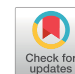

Rong-Bin Xu[a], Huan Xu[a], Yang Mei[a], Xiao-Ling Shi[a], Lei-Ying Ying[a], Zhi-Wei Zheng[a], Hao Long[a], Zhi-Ren Qiu[b], Bao-Ping Zhang[a,*], Jian-Ping Liu[c,**], Hao-Chung Kuo[a,d,e]

[a] Department of Electronic Engineering, Laboratory of Micro/Nano-Optoelectronics, School of Electronic Science and Engineering, Xiamen University, Xiamen 361005, China

[b] State Key Laboratory of Optoelectronic Materials and Technologies and School of Physics, Sun Yat-Sen University, Guangzhou 510275, China

[c] Suzhou Institute of Nano-tech and Nano-bionics, Chinese Academy of Sciences, Suzhou 215123, China

[d] Department of Photonics and Institute of Electro-Optical Engineering, National Chiao Tung University, Hsinchu 300, Taiwan

[e] Department of Electrical Engineering and Computer Sciences and TBSI, University of California at Berkeley, Berkeley, CA 94720, USA

ABSTRACT

We fabricated GaN-based blue resonant-cavity light-emitting diodes (RCLEDs) by inserting InGaN quantum well (QW) active region between two dielectric distributed Bragg reflectors (DBRs). Due to the different gain enhancement factors in a single device, multi-longitudinal modes were observed and tuned with changing the injection current density: pure-blue (PB) at low current density, violet-blue (VB) at intermediate current density, and PB again at high current density. The variation of emission spectra is explained by the competition between band-filling effect and self-heating effect.

1. Introduction

III-nitrides (GaN, InGaN, and AlGaN) have attracted an increasing interest since they are applicable to visible and ultraviolet optoelectronic devices [1–3]. GaN-based light sources including light-emitting diodes (LEDs) and laser diodes have already been commercialized and are widely applied in displays and lighting [4]. Recently, GaN-based microcavity light emitters such as resonant-cavity LEDs (RCLEDs) and vertical-cavity surface-emitting lasers (VCSELs) have attracted a lot of attention [5–10]. Compared with conventional LEDs, RCLEDs are characterized by several advantages such as high spectral purity, better emission directionality, etc. These advantages make it a potential candidate for applications such as in plastic fiber communications, mobile projectors, and free-space visible light communications [7]. In general, the structure of RCLEDs consists of two mirrors and quantum well (QW) layers for light generation. The spontaneous emission can be modified when the light emitting medium is placed inside a cavity, which is known as cavity effect [11]. However, although GaN-based RCLEDs have already been demonstrated with obvious cavity effect in the emission spectrum [5], less effort was made to study the mechanisms of spectral dynamics. Understanding the photon emission mechanisms is a key issue for further developing such optoelectronics devices.

In this work, we report the spectral tuning of blue RCLEDs. Due to the resonant cavity enhancement, the multi-longitudinal modes to resonate in the cavity with different gain enhancement factors were divided into two color groups, pure-blue (PB) and violet-blue (VB). By varying the current densities, the output wavelength can be tuned between PB and VB emitting regions. Band-filling effect and self-heating effect play dominant roles at low and high injection current densities, respectively.

2. Material and methods

The epitaxial layers of the devices were grown on a c-plane (0001) sapphire substrate using metal organic chemical vapor deposition system. The active region consisted of two layers of InGaN (2.5 nm)/GaN (6 nm) QWs and shows an emission peak at 445 nm by photoluminescence (PL), as shown in Fig. 1(a). Fig. 1(b) shows the schematic diagram of the device. To fabricate the device, an disk-shape ITO current spreading layer with a diameter of 10 μm and a SiO_2 current confinement layer were formed on the p-side wafer surface. The sapphire substrate was removed using laser lift-off after plating a thick copper layer on the surface. The bottom (13.5-pair TiO_2/SiO_2) and top (12-pair TiO_2/SiO_2) dielectric distributed Bragg reflectors (DBRs) have a reflectivity of more than 99% at the center wavelength of 440 nm. The devices were separated by ICP etching and Cr/Au was used for both p- and n-type electrodes.

* Corresponding author.
** Corresponding author.
E-mail addresses: bzhang@xmu.edu.cn (B.-P. Zhang), jpliu2010@sinano.ac.cn (J.-P. Liu).

https://doi.org/10.1016/j.jlumin.2019.116717
Received 2 April 2019; Received in revised form 20 July 2019; Accepted 21 August 2019
Available online 22 August 2019
0022-2313/ © 2019 Elsevier B.V. All rights reserved.

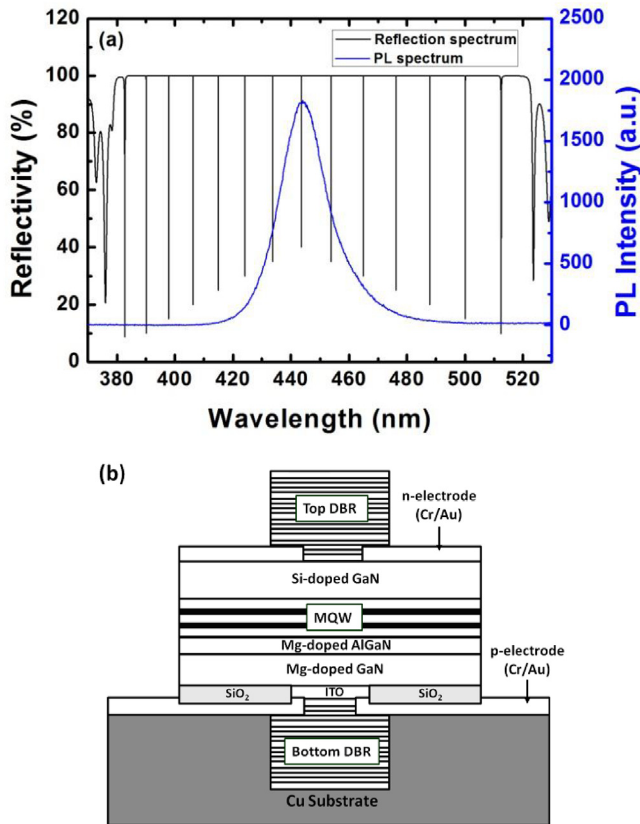

Fig. 1. (a) Measured PL spectrum of the InGaN QW sample excited by a 355 nm laser at 300 K and calculated reflection spectrum of the designed microcavity. (b) Configuration structure of the RCLEDs.

3. Results and discussion

3.1. Optical properties measured by room temperature electroluminescence

The simulation result of the reflection spectrum of the whole structure is also shown in Fig. 1(a). Because of the relatively long cavity-length and wide 150 nm DBR stop band, there are several cavity modes locating in the QW emission range. Fig. 2 presents the room temperature (RT) electroluminescence (EL) spectra measured from a device under different injection current densities. Seven cavity modes were observed in the measurement, which is consistent with the calculated result in Fig. 1(a). The cavity length calculated from the mode spacing is about 21λ. The gain of the active region is "channeled" into the cavity modes, which can greatly improve the spectral purity. Under the current density of 0.13 kA/cm^2, only two cavity modes at 454 nm and 465 nm are dominated. As the current density increases to 13 kA/cm^2, two modes at 424 nm and 433 nm are pronounced since much more carriers can be filled in high energy states. As the current density further increases to 51 kA/cm^2, the emission peak is tuned back to PB again with a small red-shift due to the heating effect.

It is known that the carrier transport among deep and shallow localized states in QWs play an important role for spontaneous emission [12,13]. To explain the observed spectral variation with injection levels, a localization model is proposed, as shown in Fig. 3. At low current densities, carriers are mainly distributed in the deep localized states due to the stronger localization and quantum confinement effect (QCE). For intermediate current densities, the carrier concentration is much higher. The band-filling effect occurs and more carriers can occupy shallow localized states, leading to a blue-shift. At high injection current densities, the carriers in the shallow localized states are thermally excited over the potential barrier. As a result, the emission returns back

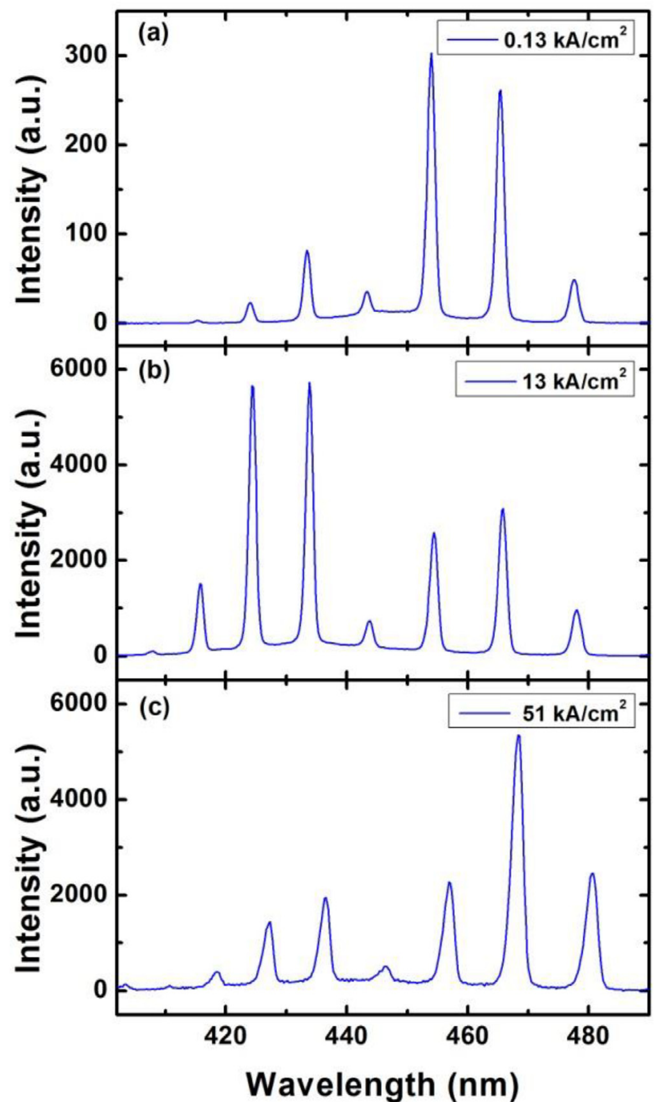

Fig. 2. EL spectra of the RCLED measured at three different current densities: (a) 0.13, (b) 13 and (c) 51 kA/cm^2, respectively.

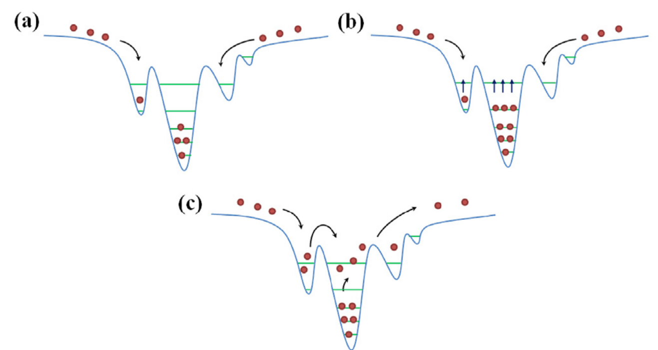

Fig. 3. Schematic diagrams indicating the possible processes of carriers transferring in the QWs at different injection levels. The carrier distributions at low current density, intermediate current density, and high current density are shown in (a), (b) and (c), respectively.

to the deep localization centers, appearing as a red-shift. This is different from our previous report where quantum dots (QDs) active region was adopted [14]. In Ref. 14, band filling or carrier accumulation was the dominant mechanism of spectral tuning.

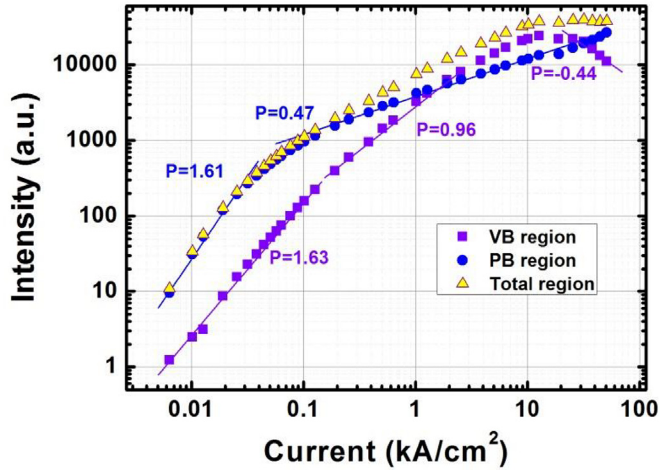

Fig. 4. Integrated EL intensity of VB, PB and total emission regions as a function of injected current density in logarithmic scale.

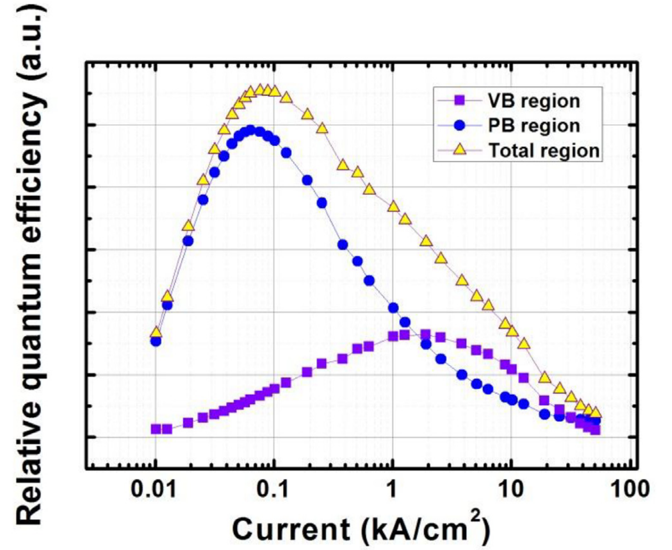

Fig. 5. Relative quantum efficiency of VB, PB and total emission regions as a function of the injected current density plotted using a logarithmic scale on the x axis.

To further investigate the different components of the EL spectra, we divide the cavity modes into two groups: the cavity modes at 415, 424 and 433 nm are defined as VB region, while the modes at 454, 465 and 478 nm are defined as PB region. The integrated intensity of VB and PB regions versus injection current density is shown in Fig. 4.

In general, the collected EL intensity is proportional to the injected current density with the power law [15].

$$L \propto J^P \tag{1}$$

where L is the integrated EL intensity, J is the current density, and P physically reflects the various recombination processes. Superlinear zone (P > 1 or < 1) and linear zone (P ~ 1) were observed with the P values were indicated in Fig. 4. Under small injection current densities (J < 0.04 kA/cm^2 for PB and J < 0.1 kA/cm^2 for VB), superlinear dependence of intensity on current density is observed for both emission bands, which suggests that the defect-related nonradiative recombination plays an important role in the low injection levels. For deep localization states, however, the better carrier localization indicates the unimportance of defect-related nonradiative recombination, resulting in a higher emission intensity in the PB band. At higher injection current densities, deep localized states, corresponding to PB, are saturated due to their smaller density of states, and more carriers can be captured by shallow localized states, corresponding to VB [12]. The almost linear dependence of the emission intensity for VB from 0.2 to 10 kA/cm^2 indicates excitonic emission with saturation of defect-related centers. For PB region, however, the sublinear (P = 0.47) dependence at the same current density range is attributed to the appearance of the new nonradiative recombination, the Auger recombination caused by the higher carrier density, since the probability of Auger process increases strongly with decreasing energy band gap and it is more dominant at high injection levels [16,17]. Gradually, the intensity of VB exceeds that of PB. With further increasing current density (J > 10 kA/cm^2), the heating effect plays an important role in the device characteristic. The negative P value (−0.44) indicates that the intensity of VB region gradually decreases, which can be explained as temperature-induced carrier escape from the shallow localization centers [16]. Since the increase of sample temperature, a redshift of the emission peak is also expected due to the temperature-induced bandgap shrinkage [18]. As a result, the PB emission becomes stronger again. Meanwhile, due to the thermal expansion of the cavity, the resonance mode also showed shift slightly to longer wavelength. For reference, the total integrated EL intensity is also provided in Fig. 4. The behavior is influenced by carrier dynamics in deep and shallow localized states.

The relative quantum efficiency of the device can be defined as integrated EL intensity divided by injection current density. In Fig. 5, the relative quantum efficiency versus current density is compared for the VB and PB regions. For PB region, the quantum efficiencies increase monotonically from low current density, reach a maximum at ~0.04 kA/cm^2, and then decrease monotonically. The increase in quantum efficiency below 0.04 kA/cm^2 is attributed to the more rapidly increasing radiative recombination rate relative to the defect-related nonradiative recombination rate. The decrease in quantum efficiency above 0.04 kA/cm^2 is attributed to Auger recombination of the injected carriers as could be gleaned from the discussion we have above. For VB region, the efficiency degradation is also observed while the rollover current density is ~3 kA/cm^2, much higher than PB region. The higher rollover current density could be attributed to the bigger density of states of shallow localized states. Auger recombination also takes effects in VB region at a much higher current density although the P value shows no significant decrease in Fig. 4. In addition, when the current density is higher than 10 kA/cm^2, a faster quantum efficiencies decrease rate in VB region is caused by the initiate of the temperature-induced carrier escape. Overall, the relative quantum efficiency of the total emitting region is mainly affected by carrier dynamics in PB region (deep localized states).

3.2. Carrier dynamics by time-resolved photoluminescence

Time-resolved photoluminescence (TRPL) of the devices without top DBR was also measured at RT to clarify the carrier dynamics within the QW, as shown in Fig. 6. The decay curves of VB and PB regions exhibit two obvious decay stages, which are relatively faster in the early stage and slower in the extended range. The decay curves can be well fitted with a double exponential function [19]:

$$I(t) = B_1 e^{-t/\tau_1} + B_2 e^{-t/\tau_2} \tag{2}$$

where τ_1 and τ_2 represent the carrier lifetime in the fast and slow decay stages, respectively. The obtained fitting results are listed in Table 1.

In general, the carrier lifetime is affected by the carrier recombination (radiative and noradiative recombination of carrier) and escape. For the TRPL of the samples without cavity, the fast decay stage is mainly due to the carriers transfer from high-energy side to low-energy side [20]. τ_1 of low-energy side is longer than that of high-energy side. However, in this study, the samples with half-cavity shows an extremely fast decay due to the cavity effect [21,22]. Both fast and slow decay stage in device with half-cavity are mainly due to the carrier

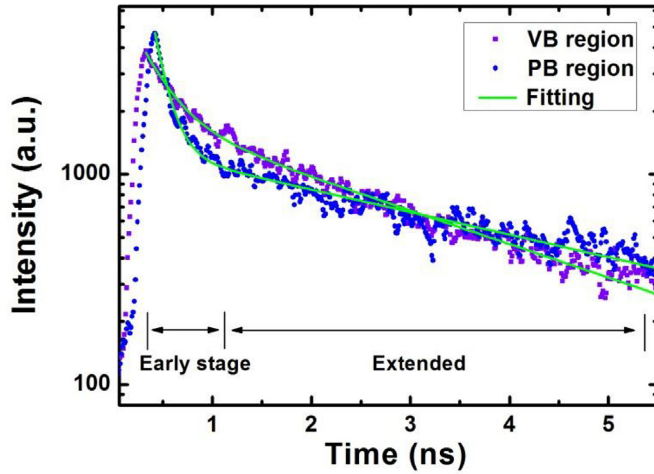

Fig. 6. TRPL curves of two emission regions.

Table 1
Carrier lifetimes at two emission regions.

Emission region	VB	PB
τ_1 (ns)	0.29	0.14
τ_2 (ns)	2.73	4.07

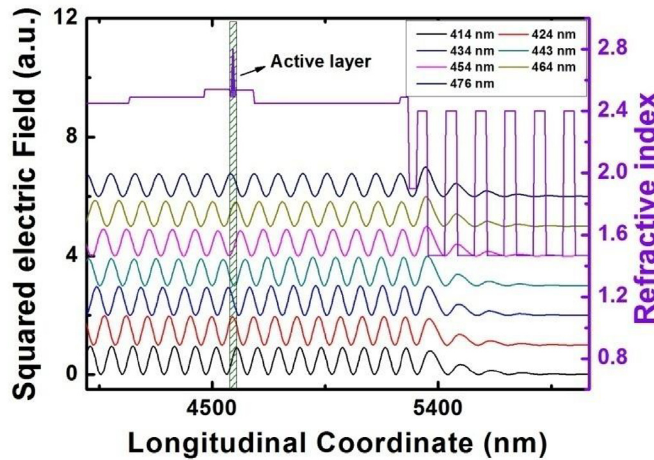

Fig. 7. The reflective index distribution of the InGaN QW RCLED and the optical field distribution for the seven cavity modes. The position of active region is filled with slant lines.

recombination, and the carrier lifetime can be expressed as [20].

$$\frac{1}{\tau} = \frac{1}{\tau_r} + \frac{1}{\tau_{nr}} \tag{3}$$

where $1/\tau_r$ and $1/\tau_{nr}$ represent the radiative and nonradiative recombination rates, respectively. Nonradiative recombination plays an important role at RT. In this modal, the two decay stages at different regions can be explained as follows: Just after the pulse excitation, where the carrier density is high, defect-related nonradiative centers are saturated. Since the deep localized states have the smaller density of states, Auger recombination caused by the high carrier density is dominant at low-energy side. Thus, τ_1 of low-energy side (PB region) is shorter than that of high-energy side (VB region), which is opposite to the samples without cavity. With the time going on, carrier density decreases. The defect-related noradiative recombination is dominant. Because of the stronger localization effects of deep localized states, the influence of defects becomes less important, resulting in a longer carrier lifetime (τ_2) in low-energy side. On the other hand, high-energy side is characterized by a shorter carrier lifetime. Such an argument is consistent with the results shown above at high and low injection currents.

Table 2
Gain enhancement factors of seven cavity modes.

Wavelength (nm)	414	424	434	443	454	464	476
Γ_r	1.1	1.61	1.01	0.15	0.44	1.41	1.52

3.3. Gain enhancement factor of emission modes

In Fig. 6, the standing wave patterns of the emission modes are calculated by the transfer matrix method. Different longitudinal modes have different gain enhancement factors (Γ_r) depending on the distribution of the optical standing waves [14]. The gain enhancement factor, defined as the optical density in the active layer normalized to that in the cavity, is given by Ref. [23].

$$\Gamma_r = \frac{L\int_{d_a}|E(z)|^2 dz}{d_a\int_L |E(z)|^2 dz} \tag{4}$$

where L, d_a, E(z) are the cavity length, thickness of the active region and optical field standing-wave pattern, respectively. The mode enhancement/suppression observed in EL spectra is attributable to the relatively high/low gain enhancement factor which can be inferred from the overlap between the active region and the standing-wave field of the seven modes, as is illustrated in Fig. 7. Γ_r of seven cavity modes is also calculated, as shown in Table 2. Γ_r varies in the range of 0–2 for different modes inside the cavity. A small gain enhancement factor of 0.15 is the main reason why the mode at 443 nm is always suppressed at different injection currents although the gain is the highest. Finally, together with the variation of gain, emission spectra of the RCLED could be tuned among the well coupled mode at different injection current densities.

4. Conclusion

In summary, we have fabricated GaN-based blue RCLEDs using InGaN QWs active layers. With increasing the injection current density, the emission is featured with three distinct evolution periods. This behavior was explained as a result of carrier accumulation and thermal activation over different localization states. The control of the gain enhancement factor for resonant cavity and the current may become an innovative approach for the mode selection. This study provides a new idea for the fabrication of color tunable devices with GaN-based QW active regions.

Acknowledgments

This work was supported in part by the Science Challenge Project (No. TZ2016003), in part by the National Key Research and Development Program of China (No. 2016YFB0400803), and in part by the National Natural Science Foundation of China (Nos. U1505253, 11474365).

References

[1] M. Koike, N. Shibata, H. Kato, Y. Takahashi, Development of high efficiency GaN-based multiquantum-well light-emitting diodes and their applications, IEEE J. Sel. Top. Quantum Electron. 8 (2002) 271–277.
[2] S. Mokkapati, C. Jagadish, III-V compound SC for optoelectronic devices, Mater. Today 12 (2009) 22–32.
[3] S. Nakamura, S.F. Chichibu, Introduction to Nitride Semiconductor Blue Lasers and Light Emitting-Diodes, CRC Press, London, 2000, p. 153.
[4] H.J. Li, P.P. Li, J.J. Kang, Z. Li, Z.C. Li, J. Li, X.Y. Yi, G.H. Wang, Phosphor-free, color-tunable monolithic InGaN light-emitting diodes, Appl. Phys. Express 6 (2013) 102103.

[5] Y.K. Song, M. Diagne, H. Zhou, A.V. Nurmikko, R.P. Schneider, Takeuchi Jr., T. Takeuchi, Resonant-cavity InGaN quantum-well blue light-emitting diodes, Appl. Phys. Lett. 77 (2000) 1744–1746.

[6] M.A. Mastro, J.D. Caldwell, R.T. Holm, R.L. Henry, C.R. Eddy Jr., Design of gallium nitride resonant cavity light-emitting diodes on Si substrates, Adv. Mater. 20 (2008) 115–118.

[7] C.C. Lin, C.T. Lee, GaN-based resonant-cavity light-emitting diodes with top and bottom dielectric distributed Bragg reflectors, IEEE Photonics Technol. Lett. 22 (2010) 1291–1293.

[8] D. Kasahara, D. Morita, T. Kosugi, K. Nakagawa, J. Kawamata, Y. Higuchi, H. Matsumura, T. Mukai, Demonstration of blue and green GaN-based vertical-cavity surface-emitting lasers by current injection at room temperature, Appl. Phys. Express 4 (2011) 072103.

[9] C.A. Forman, S.G. Lee, E.C. Young, J.A. Kearns, D.A. Cohen, J.T. Leonard, T. Margalith, S.P. DenBaars, S. Nakamura, Continuous-wave operation of m-plane GaN-based vertical-cavity surface-emitting lasers with a tunnel junction intracavity contact, Appl. Phys. Lett. 112 (2018) 111106.

[10] M. Kuramoto, S. Kobayashi, T. Akagi, K. Tazawa, K. Tanaka, T. Saito, T. Takeuchi, High-power GaN-based vertical-cavity surface-emitting lasers with AlInN/GaN distributed Bragg reflectors, Appl. Sci. 9 (2019) 416.

[11] E.F. Schubert, Y.H. Wang, A.Y. Cho, L.W. Tu, G.J. Zydzik, Resonant cavity light-emitting diode, Appl. Phys. Lett. 60 (1992) 921–923.

[12] H. Wang, Z. Ji, S. Qu, G. Wang, Y.Z. Jiang, B.L. Liu, X.G. Xu, H. Mino, Influence of excitation power and temperature on photoluminescence in InGaN/GaN multiple quantum wells, Opt. Express 20 (2012) 3932.

[13] Y.J. Yang, P. Ma, X.C. Wei, D. Yan, Y.F. Wang, Y.P. Zeng, Design strategies for enhancing carrier localization in InGaN-based light-emitting diodes, J. Lumin. 155 (2014) 238–243.

[14] Y. Mei, R.B. Xu, G.E. Weng, H. Xu, L.Y. Ying, Z.W. Zheng, H. Long, B.P. Zhang, W. Hofmann, J.P. Liu, J. Zhang, M. Li, J. Zhang, Tunable InGaN quantum dot microcavity light emitters with 129 nm tuning range from yellow-green to violet, Appl. Phys. Lett. 111 (2017) 121107.

[15] I. Martil, E. Redondo, A. Ojeda, Influence of defects on the electrical and optical characteristics of blue light-emitting diodes based on III–V nitrides, J. Appl. Phys. 81 (1997) 2442.

[16] Ü. Ozgur, H. Liu, X. Li, GaN-based light-emitting diodes: efficiency at high injection levels, P, IEEE 98 (2010) 1180.

[17] J. Piprek, Efficiency droop in nitride-based light-emitting diodes, Phys. Status Solidi A 207 (2010) 2217–2225.

[18] J.C. Lee, Y.F. Wu, Y.P. Wang, T.E. Nee, Temperature and current dependences of electroluminescence from InGaN/GaN multiple quantum wells, J. Cryst. Growth 310 (2008) 5143.

[19] L. Liu, L. Wang, N.Y. Liu, W. Yang, D. Li, W.H. Chen, Z.C. Feng, Y.C. Lee, I. Ferguson, X.D. Hu, Investigation of the light emission properties and carrier dynamics in dual-wavelength InGaN/GaN multiple-quantum well light emitting diodes, J. Appl. Phys. 112 (2012) 083101.

[20] L. Wang, Y.C. Xing, Z.B. Hao, Y. Luo, Study on carrier lifetimes in InGaN multi-quantum well with different barriers by time-resolved photoluminescence, Phys. Status Solidi (b) 252 (2015) 956–960.

[21] Y. Hou, Enhanced optical properties in a polarization-matched semiconductor plasmonic nanocavity, Mater. Lett. 236 (2019) 574–578.

[22] R.A. Taylor, A.F. Jarjour, D.P. Collins, M.J. Holmes, R.A. Oliver, M.J. Kappers, C.J. Humphreys, Cavity enhancement of single quantum dot emission in the blue, Nanoscale Res. Lett. 5 (2010) 608–612.

[23] R. Michalzik, Fundamentals, Technology and Applications of Vertical-Cavity SurfaceEmitting Lasers, Springer, Berlin, 2013, pp. 27–30.